Bulk Analysis of Tobacco and Cigarettes by Magnetic Resonance Imaging

David E. Axelson

MRI Consulting, 8 Wilmot Street, Kingston, Ontario, Canada K7L 4V1

Jan B. Wooten*

Philip Morris Research Center, P.O. Box 26583, Richmond, Virginia 23261-6583

Proton magnetic resonance imaging of tobacco blends in cigarette rods was investigated to assess the feasibility of various imaging protocols to characterize and quantify the structure and composition of multiphase plant materials in situ. The protocols used to characterize the rigid molecular components (plant cell wall) included single-point imaging (SPI) and a variant experiment, single-point ramped imaging with T_1 enhancement (SPRITE). Both 1D profiles, radially averaged along the length of a cigarette, and 2D maps of proton spin density and relaxation (T_2*) were acquired. Mobile components (tobacco waxes and water) were examined via conventional spin−echo imaging techniques, with 1D, 2D, and 3D data being acquired. Spin−spin relaxation times (T_2), apparent spin−spin relaxation (T_2*), and spin−lattice (T_1) relaxation times were measured for selected samples.

Keywords: *Tobacco; nuclear magnetic resonance (NMR); cigarettes; imaging; magnetic resonance imaging (MRI)*

INTRODUCTION

The usual cost-effective approach to the bulk analysis of materials is to make measurements of whole samples and to search for suitable correlations among the analytical data that permit product factors such as quality, processing conditions, and production costs to be optimized. Although this strategy may be generally useful, it becomes increasingly unproductive when the materials in question are complex, heterogeneous mixtures, and the processes involving their production are characterized by significant nonlinear relationships that can obscure simple correlations. If the samples are multiphase, solid materials derived from plants, such as cigarettes and many processed foods, the number of analytical methods applicable to their study is significantly limited. This is particularly true when the sample preparation involves elevated temperature, fractionation, solvent extraction, wet chemical treatment, or other procedures that are likely to alter the original chemical composition, phase relationships, or their spatial distribution. In this regard, we have investigated several very new solid-state nuclear magnetic resonance (NMR) imaging techniques that allow for selective, nondestructive analysis of phases distinguished by different degrees of molecular mobility.

The general view of the plant primary cell wall as a composite material made up of cellulose microfibrils in a matrix of hemicelluloses, pectin polysaccharides, protein, and water is well established (MacNeil et al., 1984; Fry, 1986; Wooten, 1995). The main difficulty in applying NMR techniques to the plant cell wall is the inherent chemical and physical inhomogeneity of the plant tissue. In the current study, we are interested in the characterization of the basic NMR parameters required to optimize the NMR images of cigarettes, to discriminate specific chemical phases, and to define the limitations of these techniques. Some specific goals are ultimately to devise methods for obtaining quantitative images of tobacco waxes (samples conditioned at low relative humidity), water (samples conditioned at higher relative humidity), and rigid solid images. Ideally, we also wish to obtain the respective mass fractions of distinct phases/components, spatial distributions of individual components, dimensions of individual components, and void fractions. The availability of imaging protocols that are inherently capable of quantifying the diverse phases in tobacco is of prime importance. Although spin−echo imaging methods have been readily adapted to study the mobile components in foods (Hills, 1998), the development of methods for imaging the rigid components has been more problematic. It has been demonstrated, however, that a technique known as single-point imaging (SPI) (Emid and Creyghton, 1985; Axelson et al., 1995, 1996) is an effective basis from which to study the rigid components in a variety of solids (roughly defined as having apparent spin−spin relaxation times, T_2*, of $<\sim$500 μs). More recently, a modification to the original experiment, called single-point ramped imaging with T_1 enhancement (SPRITE), has been developed and tested (Balcom et al., 1996; Beyea et al., 1998; Kennedy et al., 1998). The SPRITE pulse sequence will form the basis for many of the results to be reported here.

* Author to whom correspondence should be addressed [telephone (804) 274-3465; fax (804) 274-2160; e-mail jan.b.wooten@pmusa.com].

10.1021/jf991075t CCC: $19.00
Published on Web 05/24/2000

MATERIALS AND METHODS

Magnetic Resonance Imaging (MRI) Considerations. Given the complex nature of the materials under investigation, we make note of the numerous advantages that MRI offers for bulk analysis. First and foremost, it readily gives spatial information about a sample. Combined with time-dependent observations, MRI can be a powerful analytical tool for the characterization of dynamic processes. Furthermore, this spatial resolution can be combined with one or more image contrast mechanisms (based on concentration, composition, relaxation times, diffusion constants, flow/velocity, and molecular mobility) to provide an extremely detailed characterization of heterogeneous samples. It is therefore possible in principle to make quantitative multidimensional measurements of compositional variations as long as the nature of the relationship between the structures involved and the corresponding NMR/MRI properties to be measured is understood. Given the volume and complexity of the data, this objective may require a combination of multivariate image analysis techniques and other multivariate methods such as principal component analysis, partial least squares, and neural network analyses (Malinowski and Howery, 1980; Bishop, 1995; Ripley, 1996; Despagne and Massart, 1988).

In many respects, MRI is complementary to other imaging methods such as neutron radiography (Brenizer et al., 1987), whereas in many other respects it offers unique capabilities and opportunities. In our test examples, the plant materials under scrutiny have suitable dimensions and are spatially stable, and any dynamic change is slow, thus making cigarettes highly suitable for imaging experiments. There is an inherent relationship between the gradient strength required to achieve a given pixel resolution and the line width of the samples being imaged. Consider a spin system with a line width, $\delta\nu$, being imaged using a frequency-encoding method. The frequency separation between two neighboring voxels along the gradient direction, $\Delta\nu$, should be larger than the line width ($\Delta\nu \geq \delta\nu$). Such a requirement imposes the line width resolution limit on NMR microscopy expressed by $\Delta r \geq 2\pi\delta\nu/\gamma G$, where G is a linear magnetic field gradient in the direction of Δr. If the magnetic field is homogeneous over the sample and magnetic susceptibility effects and chemical shift effects are neglected, a Lorentzian line shape may be assumed, giving $\delta\nu = 1/\pi T_2$. Several general observations can be drawn from this simple relationship: (1) the higher the gradient strength, the better the spatial resolution inherently achievable; (2) conversely, the resolution may be limited by the available gradient strengths of the MRI system used; (3) the larger the NMR line width, the poorer the resolution achievable for a constant gradient strength; and (4) the higher the gradient strength, the larger the frequency range that must be sampled by the receiver. The digitizer resolution and bandwidth are therefore extremely important. In rigid materials, pixel resolution is generally limited in practice to values $>\sim 30-60$ μm.

For samples characterized by different line widths, we can calculate the approximate gradient strength required for imaging. Let us assume that the desired resolution, Δx, is 10 μm. Liquids and highly mobile solids with narrow line widths and T_2 of the order of 1 s require a gradient strength of $\sim$0.075 G/cm. For rubbery materials or bound fluids in porous media with T_2 of the order of 10 ms, the gradient strength required increases to $\sim$7.5 G/cm, a value well within the capabilities of most instrumentation equipped for imaging. At the other extreme, rigid solids with T_2 of the order of 60 μs (and lower) would necessitate the use of gradient strengths of $>$1250 G/cm. Such high values generally require specialized equipment and/or the use of samples of microscopic dimensions. Plant materials contain features that actually span the entire range of the values noted. For the very shortest T_2 or T_2* values expected to be encountered ($\sim$10 μs), probe limitations (dead times) must also be addressed. The present experiments were conducted at 99 or 200 MHz with gradients ranging up to 25 G/cm.

Samples. The cigarette samples were chosen without regard for manufacturer, brand, or manufacturing practice and are therefore denoted as "generic". Samples were selected to illustrate various features of the characterization process. Most samples were studied as-received, that is, at ambient moisture content, unless otherwise noted. The bright tobacco used in the hand-packed cigarette was cut bright tobacco cigarette filler. Samples were placed in the open in the various probes used and studied under equilibrium conditions of moisture and temperature. Multiple analyses of the same samples as a function of time as well as multiple samples from the same packages showed that relaxation time distributions within the samples were essentially identical.

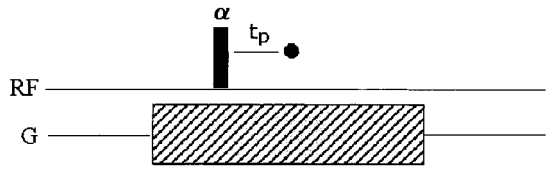

Figure 1. SPI RF pulse sequence in one dimension.

Instrumentation. Data were acquired on two instruments: (1) a Nalorac 2.4T, 32 cm horizontal bore superconducting magnet operating at 99.3 MHz with a water-cooled 20 cm i.d. self-shielded gradient set, a Tecmag Libra S-16 console, a 2 kW AMT RF amplifier, gradients driven by Techron 7780 amplifiers; and (2) a Bruker DMX200 system operating at 200.13 MHz for ^{1}H observation. In the Bruker case, the sample insert was a 10 mm NMR tube in which the sample was placed. For the low-field measurements, two inserts were used, one with a 10 cm diameter and one with $\sim$1 cm i.d.

Single-Point Imaging (SPI). In contast to the spin−echo method, the SPI sequence does not employ broadband selective pulses but relies on broadband rf pulses of limited duration as shown in Figure 1. The pulse bandwidth (1/pulse length) must be greater than the maximum spectral width ($G_{max} \times$ sample length) to ensure uniform excitation. Position is encoded in reciprocal space, $S(k)$, where $k = 1/(2\pi)\gamma Gt$, and by amplitude cycling of the applied phase gradients, G, where $t =$ gradient on time. A single point on the FID is sampled in quadrature detection at a fixed encoding time, $t = t_p$, after the RF pulse. Unlike frequency-encoded images, SPI images are free from distortions due to B_0 inhomogeneity, susceptibility variations, and chemical shift. The resolution, even for short T_2* species, is limited only by the maximum gradient that can be applied to the sample. A broadband rf pulse excites transverse relaxation, which is phase encoded for time t_p. A single complex point is acquired at each gradient value. The signal intensity, S, from any point in the image is related to local proton density, ρ, by

$$S = \rho \exp(-t_p/T_2^*)[(1 - \exp(-(\mathrm{TR})/T_1) \sin\theta)/(1 - \cos\theta \exp(-(\mathrm{TR})/T_1))] \quad (1)$$

assuming that transverse relaxation is dephased prior to RF excitation. In eq 1, TR is the pulse repetition time and θ is the RF flip angle.

The SPI sequence is often time inefficient because at least one scan for each resolution element is required. The third term of eq 1 suggests that there is a minimum acceptable value of TR for a given RF flip angle to achieve an acceptable signal. This time restriction can be avoided in certain circumstances by reducing the flip angle at the expense of the observable signal. The repetition time TR is not, however, the limiting factor in many cases. The finite time required to safely and repetitively switch magnetic field gradients can be the limiting condition. Intense, rapidly switched gradient pulses can lead to excessive gradient vibrations and heating. In response to these limitations, a ramped gradient version of the SPI sequence, SPRITE, has been developed. The modified pulse sequence greatly reduces imaging times, minimizes gradient vibration, and enables the introduction of quantitative T_1 contrast or T_1 suppression into a variety of images (Balcom et al., 1996; Beyea et al., 1998; Kennedy et al., 1998).

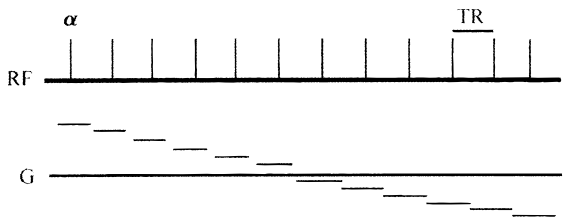

Figure 2. SPRITE pulse sequence with one gradient stepped (step length < 5 ms) with an RF pulse applied at each step. The figure shows only a few steps, although 64 or 128 are typically employed.

In the SPRITE sequence, unlike the basic SPI sequence, the gradients are not switched on or off for each acquisition. Instead, the gradient is ramped in discrete steps and an RF pulse is applied at each step, collecting a single data point as shown in Figure 2. The step length is <5 ms so that the overall gradient duration is brief and the mechanical force on the gradients is minimal (because of the low overall magnetic field drift). The phase-encoding gradients in the SPRITE sequence inherently spoil transverse magnetization. Presaturation with variable recovery time may be used as the basis of a SPRITE method to quantitatively map T_1 in samples with T_1 longer than the gradient rise time. The form of eq 1 suggests that if 90° RF pulses are applied to samples with T_1 on the order of the step duration, T_1 contrast can be introduced.

By using a long repetition time, TR, and/or small RF flip angle, θ, an image can be obtained with spin density, ρ, weighted purely by the apparent spin−spin relaxation time, T_2*. Therefore, by acquiring a series of images (typically 10−15) with variable encoding time, t_p (ranging from ∼10 to 1000 μs) and a maximum gradient strength varied so as to keep a constant field of view, we obtain a spatial map of T_2*. These data can then be analyzed using a nonlinear least-squares algorithm to account for the presence of one- or two-component decays. Each individual image requires ∼10 min to acquire so that the entire range of relevant apparent spin−spin relaxation times can be conveniently assembled in ∼2 h. This method becomes increasingly impractical (time and cost constraints) for samples with decreasing signal-to-noise ratios (and, by inference, decreasing T_2* values). Given the long time currently required for full mapping on some samples, we also employed a version of the SPRITE sequence that acquires profiles only. In this approach, the average relaxation time (T_1 or T_2*) is projected through a cross section of the sample (in our case, along either the long or short axis of the cigarette). Low flip angle pulses were employed to avoid T_1 saturation, and the gradients were adjusted to keep a constant field of view. The precise experimental parameters employed for each type of experiment are given in the corresponding relevant figure legends. All calculations were made using programs developed with IDL software (Research Systems Inc, Boulder, CO).

Spin−Echo Imaging. All data acquired by the spin−echo method used the standard CPMG data acquisition method. Detailed experimental parameters are included in the corresponding figure legends. It is important to remember that the samples were studied, unless otherwise noted, under ambient conditions, generally ∼20 °C and ambient humidity. However, natural variations in humidity and temperature might be expected to have some effect on time-dependent properties of materials that have the capacity for hydration/dehydration. These variations in turn might also be reflected in the details of the magnetic resonance parameters studied. Our goal in the present paper is to provide a general overview of the experimental possibilities as a basis for further diagnostic measurements to be made in the future.

RESULTS AND DISCUSSION

Spin−Echo Imaging. To illustrate the possibilities for the bulk analysis of tobacco, we present several different types of experiments and selected options for data visualization. Each of these methods is also relevant to the characterization and quantification of food-related materials (Hills, 1998). Because the various components in plants exhibit distinctive relaxation

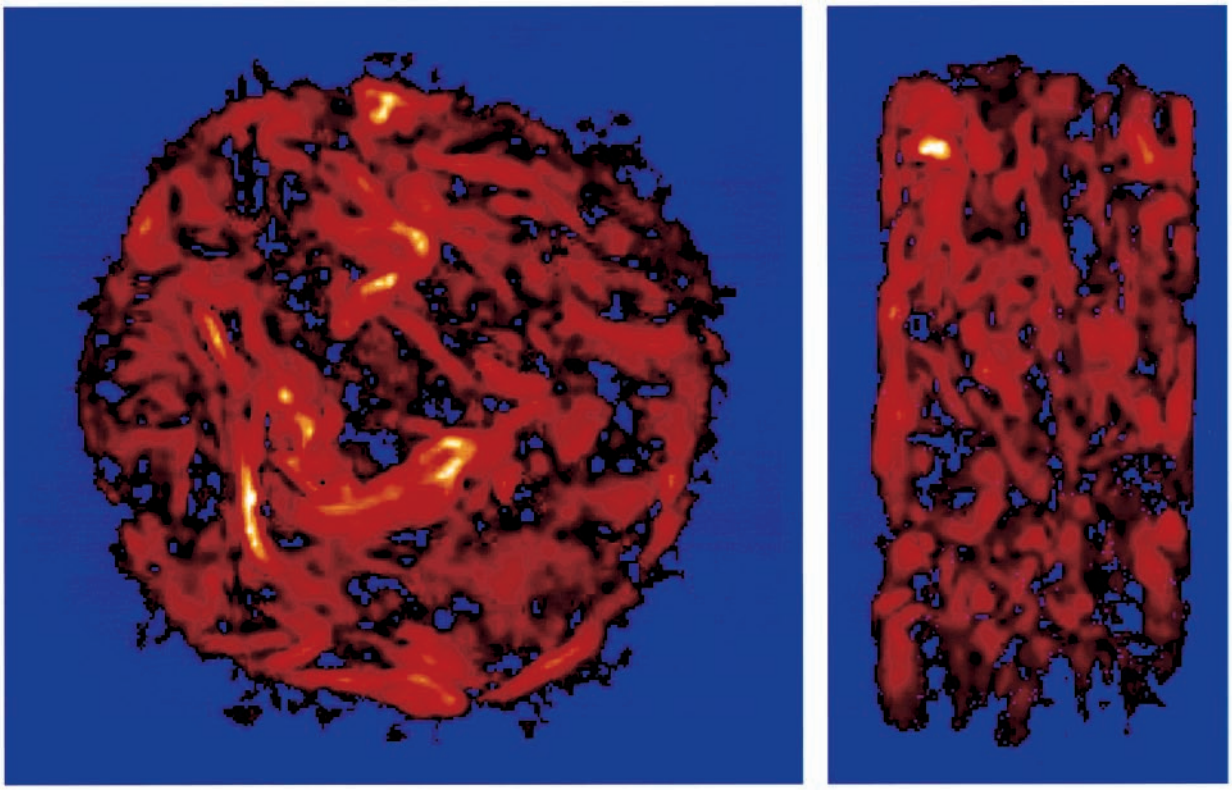

Figure 3. Transverse (left) and logitudinal (right) slices from the ^{1}H spin−echo image of a generic cigarette. Sample was kept in a high-humidity environment overnight. Field of view: 15 mm × 15 mm × 15 mm. Spatial resolution: ∼300 μm.

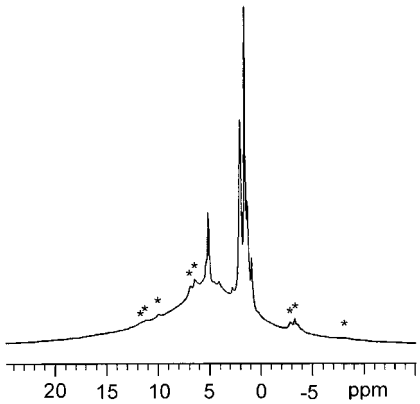

Figure 4. ^{1}H 200 MHz magic angle spinning NMR spectrum of a bright tobacco sample equilibrated at 60% relative humidity at 75 °C. Spinning side bands are denoted by *.

times dependent on their relative molecular mobilities, imaging protocols can be chosen to selectively obtain the spatial distribution of certain chemical species or phases on the basis of their relaxation behaviors. Figure 3 illustrates this in a general way. Both images were taken utilizing the spin−echo method and represent transverse and longitudinal slices through the same cigarette. The relative intensities are color-coded so that yellow is associated with the most mobile molecular species and red represents the least mobile species. Other color-coded representations can be derived to illustrate quantitative, rather than qualitative, changes in concentration. Voids and immobilized, rigid components were largely removed and appear as background in these images.

Although we are not concerned here with spectroscopy, it is important to note the relationship between the spectroscopic results and the spin−echo images shown in Figure 3. The ^{1}H 200 MHz magic angle spinning NMR spectrum of a bright tobacco sample equilibrated at 60% relative humidity at 75 °C is shown in Figure 4. The resonance line width of the water component is ~1800 Hz full width at half-height and is seen as the broad hump underneath the relatively sharp lines attributed to solanesol and other hydrocarbon waxes (Wooten, 1985). Under nonspinning conditions (as occurs in normal MRI experiments), these line widths are even greater. Generally speaking, the broadest components of a ^{1}H spectrum (e.g., bound water; rigid crystalline/amorphous polysaccharide phases) are associated with short T_2* relaxation times, whereas the narrow lines (e.g., waxes and mobile water) are associated with much longer relaxation times. Note that the signals of the rigid cell wall components and immobilized water are largely absent in Figure 4 because of their short T_2* values and the choice of acquisition parameters. Variations in sample preparation procedures, especially with respect to humidity and temperature, can lead to systematic variations in the composition. The differences in composition translate into variations in relative signal intensity in MR spin−echo images as a function of the chosen acquisition parameters.

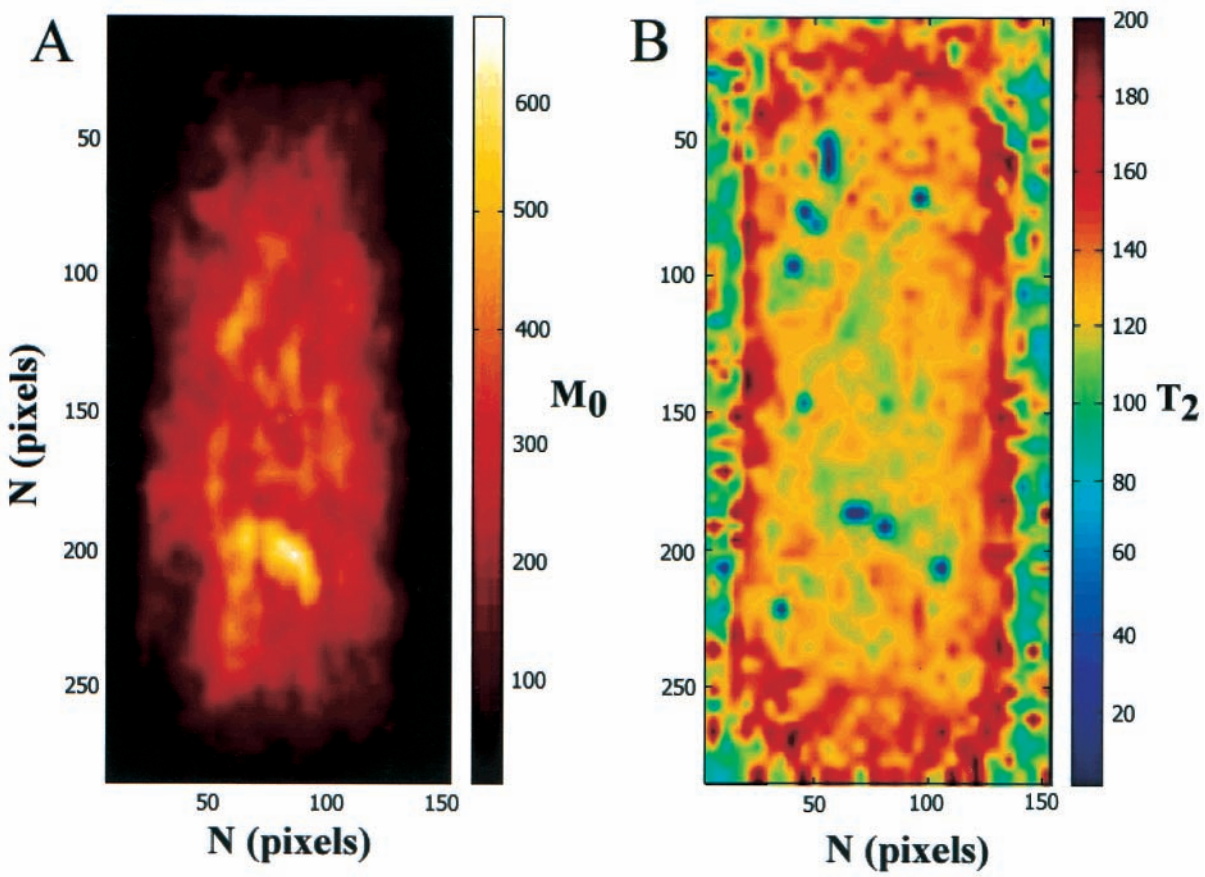

Figure 5. (A) Spin density map (M_0) derived from the SPRITE experiment for bright tobacco in a hand-packed cigarette rod. (B) T_2 map of the same sample. Experimental details: 200 MHz 2D SPRITE acquisition matrix size = 32 × 32; spectral width = 100000 Hz; pulse length = 4.7 ms; number of averages = 8; filter width = 125000 Hz; detection time = variable; repetition time = 80 ms; duty cycle = 0.33; field of view = 2.00 × 2.00 cm.

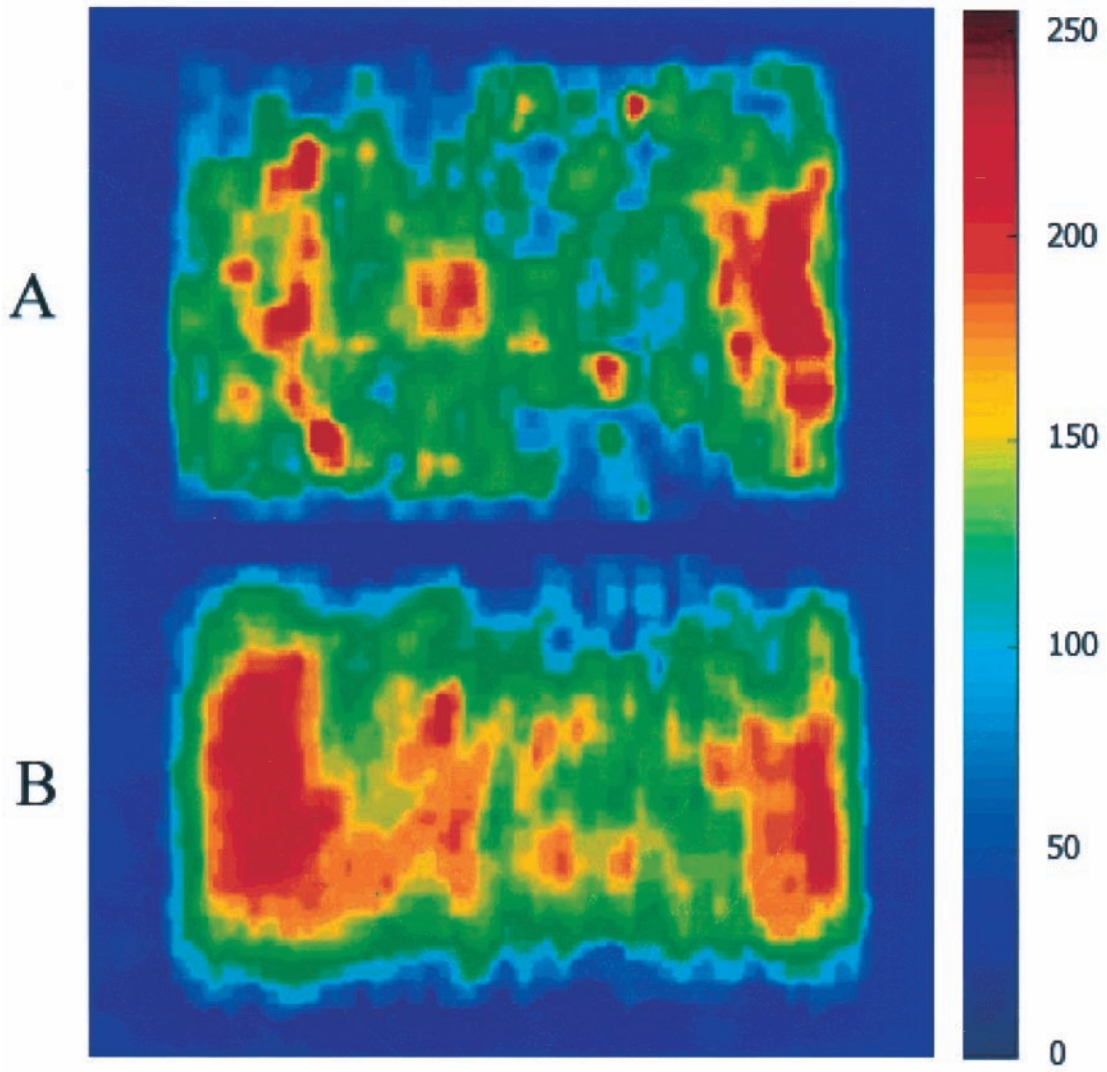

Figure 6. Spin density map derived from a spin−echo experiment for a generic cigarette equilibrated at 75% relative humidity (A) and corresponding SPRITE spin density map (B). The colors in the two images reflect relative proton concentration in each map but are not correlated with each other.

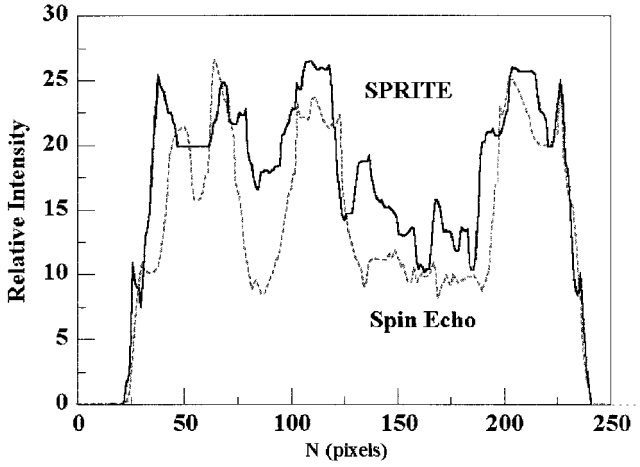

Figure 7. Longitudinal spin density profiles derived from the SPRITE experiment (solid line) and corresponding spin−echo spin density profiles (broken line) for a generic cigarette.

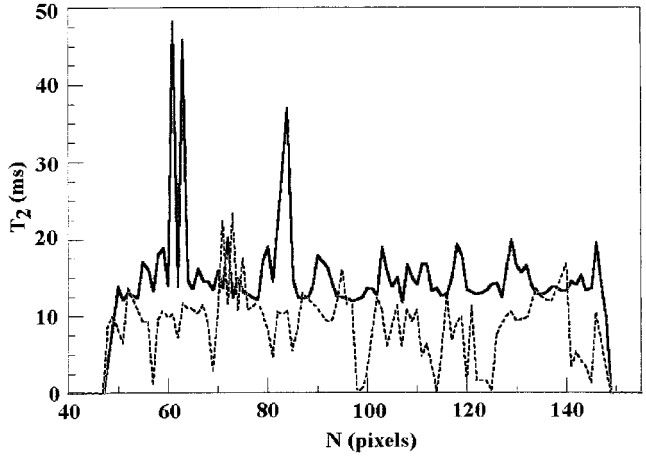

Figure 8. Spin−echo-derived two-component T_2 spin−relaxation time profiles for a generic cigarette. Experimental details: 99.3 MHz 1D spin−echo profiles (spin−spin relaxation time T_2); data points = 256; scans = 1024; spectral width = ±40000 Hz; filter width = 40000 Hz; acquisition time = 3.2 ms; dwell time = 12.5 μs; pulse width 1 = 30 ms; pulse width 2 = 60 ms; number of scans = 11; minimum echo time (TE) = 6 ms; delay values (μs) = 500, 1000, 1500, 2000, 3000, 4000, 5000, 7000, 10000, 15000, and 20000.

SPI. In contrast to spin−echo imaging, which detects plant components with the greatest molecular mobility, SPI can be used to selectively detect the least mobile components. In a wide-line ^{1}H NMR experiment, these

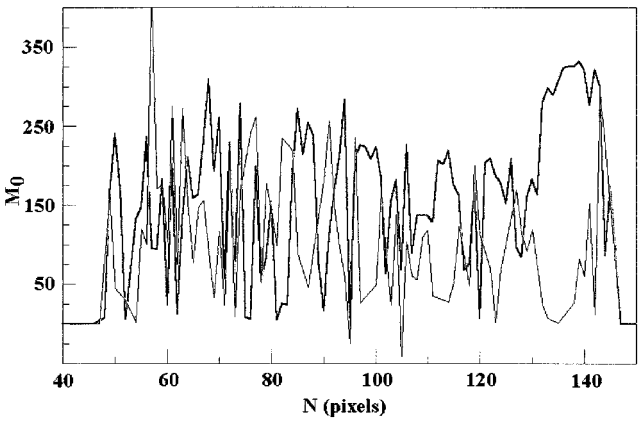

Figure 9. Spin−echo-derived two-component spin density profiles (M_0) for a generic cigarette.

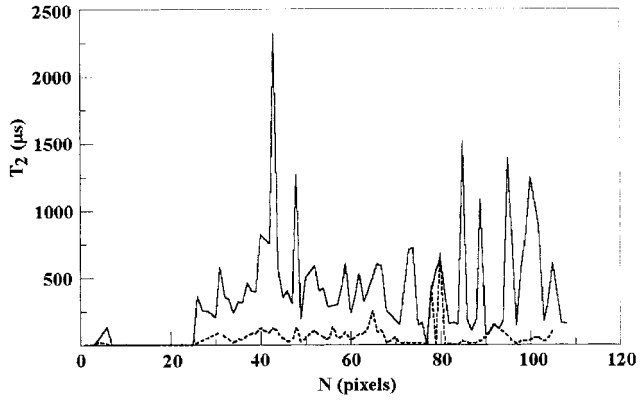

Figure 10. SPRITE-derived two-component T_2* spin−relaxation time profiles for a generic cigarette. Experimental details: 99.3 MHz 1D SPRITE profile T_2*; data points = 128; number of scans = 64; spectral width = ±125000 Hz; filter width = ±40000 Hz; acquisition time = 512 ms; dwell time = 4 μs; pulse width = 30 ms; delay values (μs) = 75, 100, 125, 150, 175, 200, 250, 300, 350, 400, 450, 500, 600, 700, 800, and 1000.

components exhibit the most rapidly decaying time domain signals (T_2* values of the order of 10 μs, for instance) and the broadest resonances in the frequency domain spectrum. For the most part, the motionally restricted components consist of the cell wall polysaccharides and other polymers, but, for desiccated samples, may also include any polycrystalline or glassy organic solids. Provided that the instrument dead time is sufficiently short to observe all of the rapidly decaying signals and the signal-to-noise ratio is sufficiently high, it is possible to acquire a full two-dimensional image as a function of phase encoding time. This experiment, which resembles a conventional CPMG spin−echo experiment for measuring T_2, can yield a map of spatially distinct spin−spin relaxation times for each picture element of the MR image. Moreover, by combining the imaging and relaxation measurements, a spin density map (image) can be constructed that is essentially free of intensity distortions due to incomplete relaxation and thus can provide quantitative information about the sample.

To illustrate these features, a series of ^{1}H SPRITE images was obtained of a hand-packed cigarette containing cut bright tobacco. The spin density map derived from the CPMG T_2 imaging experiment is shown in Figure 5A. The T_2* map itself is given in Figure 5B. In Figure 5A, the brightest colors correspond to the most densely packed regions in the sample. The T_2* map in Figure 5B shows that the distribution of relaxation times for such samples is particularly homogeneous. Nevertheless, a distinctive border appears on the periphery of the sample. This effect has been observed in other kinds of samples and apparently is a consequence of the alteration of the T_2 of the tobacco closest to the outside due to hydration effects.

By applying the spin−echo and SPRITE methods in tandem on the same sample, an important feature of MRI for the bulk analysis of plant materials becomes apparent. Figure 6 illustrates this feature for a machine-packed, generic cigarette equilibrated at 75% relative humidity. When the spin density maps obtained by the two experiments are viewed side by side, a gross distinction can be made between the "very mobile" (Figure 6A) and "immobile" (Figure 6B) components inside the cigarette. Figure 6 demonstrates how water in the sample can be mapped independently of the packing density of the cigarette rod. Because the SPRITE image measures the rigid cell wall components, the image reflects the true packing of the tobacco in the cigarette rod, whereas the spin−echo image shows the regions of highest mobile proton concentration. In the case of a hydrated cigarette, as in Figure 6A, the spin−echo image is dominated by water. The SPRITE image in Figure 6B reveals that the tobacco is more densely packed at the tip end of the cigarette than in the middle. This result is consistent with the common manufacturing practice of packing more tobacco into the tip of the cigarette to prevent the shreds from falling out of the rod. The spin−echo image (Figure 6A), on the other hand, shows that the tobacco at the tip end is drier than tobacco a few millimeters inside the rod due to exposure to the outside. Similarly on the filter end, the SPRITE image shows a greater tobacco packing density than in the center of the rod, whereas the spin−echo image shows that water has been drawn out of the rod by the cellulose acetate filter and is concentrated in a small region close to the filter.

Because the different tobacco components in a cigarette blend differ in their water activities, the edge boundaries of the individual shreds in the spin−echo image are not uniformly distinct. By comparing the spin−echo image to the SPRITE image of the same cigarette, however, the spatial distribution of water inside the cigarette can be mapped onto the more distinct boundaries revealed by the rigid cell wall components. Thus, the practical issue of dehydration can be addressed more precisely than by applying spin−echo imaging alone.

One-Dimensional Profiling. In some instances, it may not be practical or desirable to obtain a full two-dimensional map of a sample. This situation might arise, for example, if the potential information content of a high-resolution map does not warrant the time or cost of a protracted image acquisition or if the instrument duty cycle might result in unwanted sample heating. Similarly, a 1D profile would be sufficient if the radial distribution of species to be imaged in the sample was less important than the longitudinal heterogeneity one wishes to observe. In such cases we can choose to obtain an averaged one-dimensional profile along an arbitrarily chosen dimension (in our example, the long axis of a cigarette), instead of a two-dimensional image. A one-dimensional profile in many cases can sufficiently characterize the heterogeneity of a

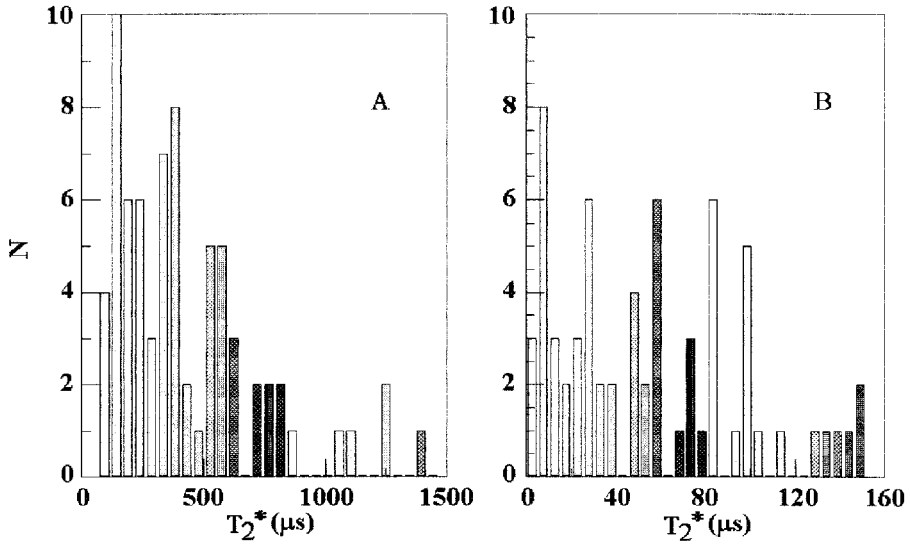

Figure 11. SPRITE two-component T_2* relaxation time histograms derived from the T_2 profile experiment for a generic cigarette: (A) long T_2* component; (B) short T_2* component.

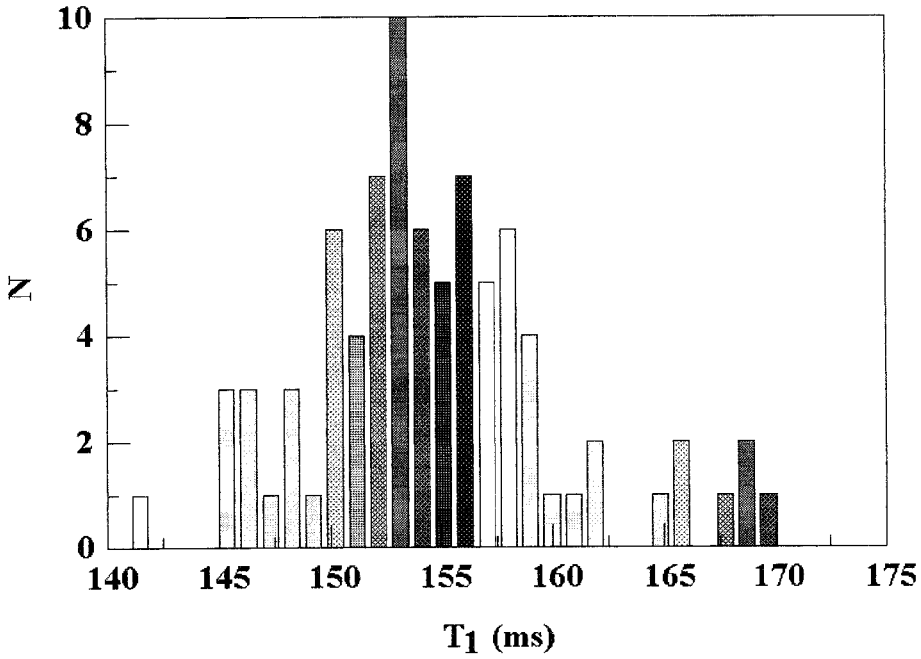

Figure 12. ^{1}H T_1 histogram for a generic cigarette obtained from an inversion−recovery T_1 experiment by spin−echo imaging. Experimental details: 99.3 MHz 1D spin−echo profile (inversion−recovery, T_1); data points = 256; scans = 512; spectral width = ±40000 Hz; filter = 40000 Hz; acquisition time = 3.2 ms; dwell time = 12.5 ms; pw (90) = 30 ms; pw (180) = 60 ms; echo time = 5 ms; delay values (ms) = 0.1, 1, 2, 3, 4, 7, 10, 15, 20, 25, 30, 40, 50, 70, 100, 130, 160, 200, 250, 300, 350, 400, 450, and 500.

sample and provide a method that is simpler and faster than full two-dimensional imaging. Profiles of both the equilibrium intensity (spin density, M_0) and the corresponding spin−spin relaxation time can be obtained from an appropriate relaxation time experiment. The utility of one-dimensional profiling is illustrated in Figure 7 for the spin−echo and SPRITE images appearing in Figure 6. Although the dimensionality of the images has been reduced, the SPRITE image profile still reflects the packing density of the cigarette and the spin−echo profile accurately shows regions of higher moisture. The values for M_0 and T_2 were obtained by assuming that the spin−spin relaxation is characterized by a single-exponential decay.

Multicomponent Relaxation. The single-component exponential decay employed to obtain the spin density profiles in Figure 7, although clearly adequate, revealed systematic differences in the relaxation curves, which indicated that a two-component fit would be more suitable. This is the expected result, rather than the exception, because multiexponential relaxation is commonly observed in complex composite materials and a number of plant constituents and cell wall components exhibit multiexponential relaxation. On a slower time scale, three different states of bonded water have been detected by NMR in pure cellulose (Mackay et al., 1985; Peemoeller and Sharp, 1985; Radloff et al., 1996). There is adsorbed water that cannot be removed from the cellulose matrix, and there is an equilibrium between rigid amorphous water and highly mobile isotropic water, which changes with temperature and depends on the water content of the sample. Multiexponential

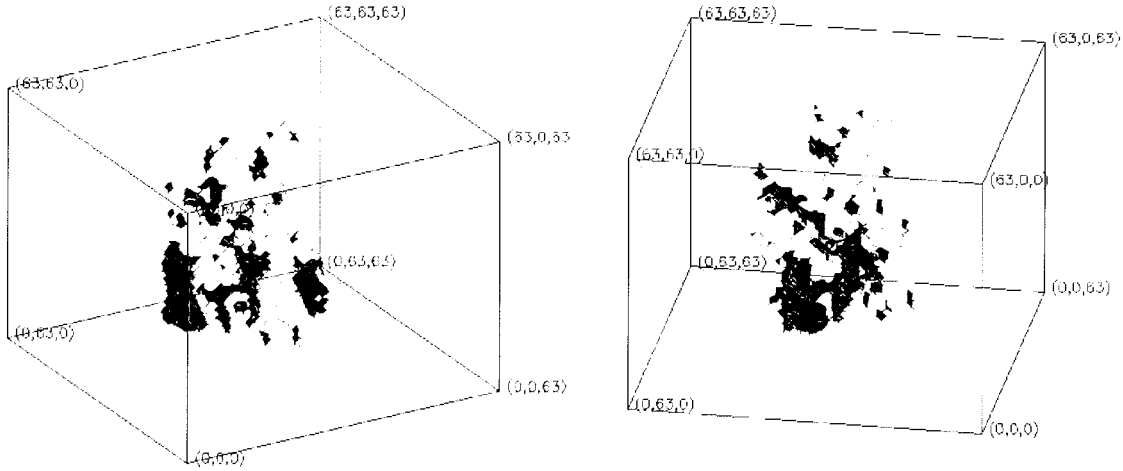

Figure 13. Three-dimensional spin−echo image of a generic cigarette at two rotational orientations of the cigarette showing regions of highest water content. The long axis of the cigarette lies along the vertical axis of each image. Experimental details: 200 MHz 3D spin−echo image; matrix size = 64 × 64 × 64; field of view, 15 mm × 15 min × 15 mm.

relaxation has also been previously observed in tobacco (Sakamoto and Nakanishi, 1996) and other plant cell walls (Mackay et al., 1982, 1988; Taylor et al., 1983, 1990).

Figures 8 and 9 show the one-dimensional profiles for the two component relaxation times (T_{2a} and T_{2b}) and spin density components (M_{0a} and M_{0b}), respectively, obtained by the spin−echo method in the test cigarette. For the majority of data points, the two-component fit to the relaxation data gave improved values of the correlation coefficient, r^2 (typically >0.99). That both components in the spin density profile in Figure 9 are almost uniform across most of the length of the cigarette reflects the fact that the sample was equilibrated at ambient relative humidity. The component corresponding to the longer T_2 (red) is clearly greater toward the filter end (right side of the figure). The dominant long T_2 component in a cigarette at ambient room hydration is solanesol (see ^{1}H MAS spectrum, Figure 4). It is not apparent, however, why solanesol should concentrate at the end of the rod near the filter (or anywhere). The greater resonance intensity might instead be due to other mobile components, but this possibility has not yet been investigated. The corresponding SPRITE T_2* two-component profiles were made on the same sample (Figure 10). Although not obvious from the behavior of the profiles as a function of dephasing time, a two-component fit was found to be most appropriate. The corresponding histogram plots (Figure 11) show that the arithmetic mean of the long component is of the order of 528 μs (464 standard deviation) and that of the shorter component ~51 μs (39.7 standard deviation). The relatively large standard deviations reflect the inherent heterogeneity of the sample components.

Although several of the points in the T_2 profiles in Figures 8 and 10 appear to be unrealistic, we include these in the results to emphasize that multicomponent analysis, involving nonlinear least-squares fitting routines, may periodically lead to "rogue" data points. These data could be recalculated using different starting values, but this might lead to a different set of points assuming unusual values. For the most consistent results, one can impose various selection criteria (data preprocessing) concerning the relative signal-to-noise ratio of the data points being used in the calculation. Although this may significantly reduce the total number of pixels used in deriving the various maps, the resulting numbers should be more reliable and representative. It is our experience that calculations should be performed with varying initial criteria for equilibrium intensities and relaxation times and that correlation coefficient and standard deviation maps can be used effectively to judge the quality of the fitted data. It should be noted that the signal-to-noise ratios in images of rigid solids tend to be significantly lower (at least an order of magnitude) than those typically encountered in spin−echo-related imaging of nonviscous solutions and even medical imaging. This imposes an additional constraint on the capability to quantify data from imaging materials of the type investigated here.

***T*$_1$ Inversion−Recovery.** For the sake of completeness, we note the data in Figure 12 concerning the spin−lattice relaxation times associated with the generic cigarette under investigation. The spin density profiles for a machine-packed cigarette were obtained as a function of inversion−recovery time. It is apparent from the T_1 values obtained from these profiles that the sample is well described by a relatively narrow range of spin−lattice relaxation times, which is confirmed in the histogram plot shown in Figure 12. Spin−lattice relaxation times of hydrated tobacco cut-fillers were previously measured by ^{1}H NMR by Sakamoto and Nakanishi (1996). The relaxation times of adsorbed water that they reported were expressed by a single-phase system of <70% relative humidity, whereas a two-phase system was applicable to water adsorbed at >80% relative humidity. Two-component fits were reported for bright tobacco T_1 (98−262 and 16−28 ms) and burley tobacco T_1 (63−172 and 15−23 ms). Our data indicate a relatively narrow distribution of relaxation times that are well characterized by a single-component decay.

3D Imaging. Three-dimensional images were acquired on a generic cigarette that had been pretreated for 24 h in a sealed container over a reservoir of water. The water was readily imaged using conventional spin−echo imaging methodologies with echo times of ~5 ms. Data were then processed with the IDL program to produce 3D ray-traced images from which image segmentation was used to isolate the most mobile (high intensity) fraction. Selected images from the 3D series are shown in Figure 13, illustrating the spatial distribution of the regions with the highest water content.

Conclusions. The complex composition and multiphase structure of tobacco (and other plant-based materials) affords a number of useful strategies for modern MRI experiments. These strategies rely primarily on the well-known capability of NMR to distinguish molecular components based on their relative mobility. The spin−echo technique, the most widely applied imaging methodology, can be readily employed to map the most mobile components, water and tobacco waxes, inside an intact cigarette. By combining spin−echo imaging with relaxation measurements and data fitting, one-, two-, and three-dimensional maps can be constructed that further discriminate among different mobile components having distinguishable resonance line widths. The most rigid components, such as the plant cell wall polymers, are amenable to imaging by the more recently developed SPI and SPRITE methods.

ACKNOWLEDGMENT

We thank Drs. Bob Ferguson, Robin Kinser, Jane Lewis, and Richard Cox for their support of this research.

Supporting Information Available: Rotating animation of the image presented in Figure 13. This material is available free of charge via the Internet at http://pubs.acs.org.

LITERATURE CITED

Axelson, D. E.; Kantzas, A.; Eads, T. Single Point ^{1}H Magnetic Resonance Imaging of Rigid Solids. *Can. J. Appl. Spectrosc.* **1995**, *40*, 16−26.

Axelson, D. E.; Kantzas, A.; Nauerth, A. ^{1}H Magnetic Resonance Imaging of Rigid Polymeric Solids. *Solid-State Nucl. Magn. Reson.* **1996**, *6*, 309−321.

Balcom, B. J.; MacGregor, R. P.; Beyea, S. D.; Green, D. P.; Armstrong, R. L.; Bremner, T. W. Single Point Ramped Imaging With T1 Enhancement (SPRITE). *J. Magn. Reson.* **1996**, *A123*, 131−134.

Beyea, S. D.; Balcom, B. J.; Prado, P. J.; Cross, A. R.; Kennedy, C. B.; Armstrong, R. L.; Bremner, T. W. Relaxation Time Mapping of Short T2* Nuclei with Single Point Imaging (SPI) Methods *J. Magn. Reson.* **1998**, *135*, 156−164.

Bishop, C. M. *Neural Networks for Pattern Recognition*; Oxford University Press: Oxford, U.K., 1995.

Brenizer, J. S.; Sulcoski, M. F.; Jenkins, R. W.; McRae, D. D.; Newman, R. H. Observations of Density Variations in Tobacco Rods by Neutron Radiography. *Beitr. Tabakforsch.* **1987**, *14*, 21.

Despagne, F.; Massart, L. Neural Networks in Multivariate Calibration. *Analyst* **1988**, *123*, 157R−178R.

Emid, S.; Creyghton, J. H. N. High-Resolution NMR Imaging in Solids. *Physica B (Amsterdam)* **1985**, *128*, 81.

Fry, S. C. Cross-Linking of Matrix Polymers in the Growing Cell-Walls of Angiosperms. *Annu. Rev. Plant Physiol.* **1986**, *37*, 164.

Hills, B. *Magnetic Resonance Imaging in Food Science*; Wiley: New York, 1998.

Kennedy, C. B.; Balcom, B. J.; Mastikhin, I. V. Three-Dimensional Magnetic Resonance Imaging of Rigid Polymeric Materials Using Single Point Ramped Imaging with T1-Enhancement (SPRITE) *Can. J. Chem.* **1998**, *76*, 1753−1765.

MacKay, A. L.; Bloom, M.; Tepfer, M.; Taylor, I. E. P. Broadline Proton Magnetic Resonance Study of Cellulose, Pectin, and Bean Cell Walls. *Biopolymers* **1982**, *21*, 1521.

MacKay, A. L.; Tepfer, M.; Taylor, I. E. P.; Volke, F. Proton nuclear magnetic resonance moment and relaxation study of cellulose morphology. *Macromolecules* **1985**, *18*, 1124.

Mackay, A. L.; Wallace, J. C.; Sasaki, K.; Taylor, I. E. P. Investigation of the Physical Structure of Primary Plant Cell Wall by Proton Magnetic Resonance. *Biochemistry* **1988**, *27*, 1467.

MacNeil, M.; Darvill, A. G.; Fry, S. C.; Albersheim, P. Structure and function of the primary cell walls of plants. *Annu. Rev. Biochem.* **1984**, *53*, 625.

Malinowski, E. R.; Howery, D. G. In *Factor Analysis in Chemistry*; Wiley-Interscience: New York, 1980.

Peemoeller, H.; Sharp, A. R. NMR study of cellulose-water systems: water proton spin−lattice relaxation in the rotating reference frame. *Polymer* **1985**, *26*, 859.

Radloff, D.; Boeffel, C.; Spiess, H. W. Cellulose and Cellulose/Poly(vinyl alcohol) Blends. 2. Water Organization revealed by Solid-State NMR Spectroscopy. *Macromolecules* **1996**, *29*, 1528.

Ripley, B. D. In *Pattern Recognition and Neural Networks*; Cambridge University Press: Cambridge, U.K., 1996.

Sakamoto, K.; Nakanishi, Y. Spin−lattice Relaxation in the Proton NMR of Hydrated Tobacco Cut-fillers. *Biosci., Biotechnol., Biochem.* **1996**, *60*, 1868.

Taylor, I. E. P.; Tepfer, M.; Callaghan, P. T.; MacKay, A. L.; Bloom, M. Use of ^{1}H NMR to study molecular motion in cellulose, pectin, and bean cell walls. *J. Appl. Polym. Sci., Appl. Polym. Symp.* **1983**, *37*, 377.

Taylor, I. E. P.; Wallace, J. C.; MacKay, A. L.; Volke, F. Use of Chemical Fractionation and Proton Nuclear Magnetic Resonance to Probe the Physical Structure of the Primary Plant Cell Wall. *Plant Physiol.* **1990**, *94*, 174.

Wooten, J. B. Direct Detection of Solanesol in Tobacco by ^{1}H and ^{13}C Magic Angle Spinning NMR. *J. Agric. Food Chem.* **1985**, *33*, 419.

Wooten, J. B. ^{13}C CPMAS NMR of Bright and Burley Tobaccos. *J. Agric. Food Chem.* **1995**, *43*, 2858.

Received for review September 29, 1999. Revised manuscript received March 15, 2000. Accepted March 29, 2000.

JF991075T